scientific reports

OPEN

Altered neurovascular coupling and structure-function coupling in Moyamoya disease affect postoperative collateral formation

Lingji Jin[1,2,5], Junwen Hu[1,2,5], Yin Li[1,2], Yuhan Zhu[1,2], Xuchao He[1,2], Ruiliang Bai[3,4] & Lin Wang[1,2]✉

Chronic ischemia in moyamoya disease (MMD) impaired white matter microstructure and neural functional network. However, the coupling between cerebral blood flow (CBF) and functional connectivity and the association between structural and functional network are largely unknown. 38 MMD patients and 20 sex/age-matched healthy controls (HC) were included for T1-weighted imaging, arterial spin labeling imaging, resting-state functional MRI and diffusion tensor imaging. All patients had preoperative and postoperative digital subtraction angiography. Upon constructing the structural connectivity (SC) and functional connectivity (FC) networks, the SC-FC coupling was calculated. After obtaining the graph theoretical parameters, neurovascular coupling represented the spatial correlation between node degree centrality (DC) of functional networks and CBF. The CBF-DC coupling and SC-FC coupling were compared between MMD and HC groups. We further analyzed the correlation between coupling indexes and cognitive scores, as well as postoperative collateral formation. Compared with HC, CBF-DC coupling was decreased in MMD ($p=0.021$), especially in the parietal lobe ($p=0.047$). SC-FC coupling in MMD decreased in frontal, occipital, and subcortical regions. Cognitive scores were correlated with the CBF-DC coupling in frontal lobes ($r=0.394$, $p=0.029$) and SC-FC coupling ($r=0.397$, $p=0.027$). The CBF-DC coupling of patients with good postoperative collateral formation was higher ($p=0.041$). Overall, neurovascular decoupling and structure-functional decoupling at the cortical level may be the underlying neuropathological mechanisms of MMD.

Keywords Cerebral blood flow, Functional connectivity, Structural connectivity, Graph theory, Moyamoya disease, Collateral formation

Abbreviations

MMD	Moyamoya disease
HC	Healthy controls
ASL	Arterial spin labeling imaging
fMRI	Functional magnetic resonance imaging
DTI	Diffusion tensor imaging
CBF	Cerebral blood flow
DSA	Digital subtraction angiography
DC	Degree centrality
SC	Structural connectivity
FC	Functional connectivity
ALFF	Amplitude of low frequency fluctuation
FA	Fractional anisotropy
NVC	Neurovascular coupling

[1]Department of Neurosurgery, The Second Affiliated Hospital, Zhejiang University School of Medicine, Jiefang Road 88th, Hangzhou 310009, China. [2]Clinical Research Center for Neurological Diseases of Zhejiang Province, Hangzhou, China. [3]Key Laboratory of Biomedical Engineering of Education Ministry, College of Biomedical Engineering and Instrument Science, Zhejiang University, Hangzhou, China. [4]MOE Frontier Science Center for Brain Science and Brain-Machine Integration, School of Brain Science and Brain Medicine, Zhejiang University, Hangzhou, China. [5]These authors contributed equally. ✉email: dr_wang@zju.edu.cn

T1WI	T1-weighted imaging
MMSE	Mini-Mental State Examination
MoCA	Montreal Cognitive Assessment
ROI	Regions of interest
AAL	Automatically labeled template
MNI	Montreal Neurological Institute
FDR	False discovery rates

Moyamoya disease (MMD) is a rare cause of stroke, radiologically characterised by progressive stenosis of the terminal portion of the internal carotid arteries and compensatory capillary collaterals[1]. Functional magnetic resonance imaging (fMRI) has the capability to reveal brain neuronal activity, thereby elucidating the cognitive impairments intertwined with neurological disorders, all through the lens of neuropathology. Previous studies based on fMRI have identified alterations in functional connectivity (FC), regional homogeneity, and amplitude of low frequency fluctuation (ALFF) in MMD, proposing an extensive reorganization of functional network[2–4]. Diffusion tensor imaging (DTI) can reflect the intricate modifications occurring in white matter fibers. Previous investigations have showed that detrimental effects of MMD on crucial fiber tracts and white matter microstructure[5–7]. Graph theory has emerged as a powerful tool for assessing the topological properties of complex functional and structural networks, and has extended to a variety of neurological disorders[8,9].

Previous studies on graph theory suggested that the functional and structural network properties of certain brain regions declined in MMD[10,11]. It is worth exploring the potential restoration of normal function in these affected regions following revascularization surgery, because perfusion restoration may not synchronize with neuronal activity. Although based on the neurovascular coupling (NVC) hypothesis that neuronal activity is closely linked to blood supply[12,13], the chronic ischemia, collateral circulation formation, and stroke in MMD may disrupt neurovascular homeostasis. Besides, neurovascular decoupling may result in alterations in the local neuronal structure and ion gradients to match the low metabolic demands of neural activity, leading to impaired vascular smooth muscle function such as dilation and extension[14–16]. Thus, the NVC decrease may also lead to poor collateral formation and perfusion restoration after revascularization in MMD[17]. Moreover, the NVC decrease can lead to cognitive decline[18,19].

Previous studies on multimodal connectivity networks have revealed a correspondence between structural connectivity (SC) and functional connectivity (FC)[20,21]. SC-FC coupling characterizes the brain functional dynamics in relation to structural topology, enabling the detection of more subtle impairment. Indeed, SC-FC coupling has been found to be linked to cognitive and executive functions in various neurological disorders[21–23]. Besides, impairments in white matter microstructure and myelin can also impact regional NVC in MMD[24,25].

However, there is a lack of studies on the NVC and SC-FC coupling in MMD. Thus, we aimed to address the following questions: Whether the NVC and SC-FC coupling change in MMD; Whether these changes affect cognitive function; Whether the NVC affects the postoperative collateral formation.

Methods
Participants
The human research ethics committee approved the study protocol, and informed consent was obtained from each subject before participation. A cohort of 38 patients with MMD was finally included from July 2020 to May 2023. All patient diagnoses of MMD were based on the digital subtraction angiography (DSA). Inclusion criteria were as follows: completed preoperative multimodal MRI data collection; right-handed; not in the acute phase of ischemia or hemorrhage. Exclusion criteria were as follows: incomplete MRI data, the MRI data not consistent with the acquisition protocol, lack of DSA data after combined bypass surgery, cortical lesions on T1-weighted imaging (T1WI) larger than 3 mm (Fig. S1). Besides, the control group consisted of 20 healthy controls (HC) with gender, age, and education matched with the MMD group. Inclusion criteria for the HC group was no history of neurologic or systematic diseases, and the exclusion criteria was macroscopic brain lesions on T1WI.

Digital subtraction angiography (DSA) before and nearly 1 year after combined bypass surgery were collected for all patients. Suzuki stage and Matsushima grade were assessed by two experienced neurosurgeons (Y Li and J Hu). Matsushima grade 1 was defined as the revascularization of $< 1/3$ of the middle cerebral artery (MCA) distribution, grade 2 as the revascularization of 1/3 to 2/3 of MCA distribution, and grade 3 as the revascularization of $> 2/3$ of MCA distribution. MMD patients were further divided into poor collateral formation group (Matsushima grade 1) and good collateral formation group (Matsushima grade 2–3). The neuropsychologic assessment was performed in MMD patients, including the Mini-Mental State Examination (MMSE) and the Montreal Cognitive Assessment (MoCA), and then cognitive scores were used for education correction.

MRI data acquisition
The study was completed on a 3T MR scanner (Discovery MR750, GE) with an 8-channel head coil. The entire protocol included T1WI, pseudo-continuous arterial spin labeling (ASL) fMRI and DTI. The total scan time for each subject was about 30 min. Earplugs and spongy padding were used to reduce the noise and head motion.

T1WIs were collected through 3D fast spoiled gradient-echo: repetition time (TR) = 7.4ms, echo time (TE) = 3.1ms, flip angle = 8°, field of view (FOV) = 256 mm × 256 mm, slices = 170, and voxel size = 0.8 mm × 0.8 mm × 1.0 mm. T2-FLAIR were acquired with following parameters: TR = 8400 ms, TE = 145.3ms, flip angle = 90°, FOV = 512 mm × 512 mm, slices = 40, and voxel size = 0.39 mm × 0.39 mm × 4.0 mm.

ASL images without vessel suppression used the following parameters: TR = 4825 ms, TE = 10.6 ms, flip angle = 111°, FOV = 128 mm × 128 mm, slices = 34, voxel size = 1.56 mm × 1.56 mm × 4.0 mm, post-labeling delay (PLD) = 1500 ms.

Resting-state fMRI was performed by using echo-planar imaging sequence with the following parameters: TR = 2002 ms, TE = 30 ms, flip angle = 77°, FOV = 218 mm × 218 mm, slices = 38, voxel size = 3.44 mm × 3.44 mm × 4.0 mm, and 180 continuous functional volumes were scanned.

DTI was acquired using 60 diffusion gradient directions with the b-values of 2,000 s/mm2 and two repetitions on b = 0 s/mm2, TR = 9000ms, TE = 92.7ms, flip angle = 90°, FOV = 256 mm × 256 mm, slices = 68, and voxel size = 1.0 mm × 1.0 mm × 2.0 mm. To correct the image distortion, we also obtained reverse phase-coded images.

FC network construction

Resting-state fMRI data were preprocessed using GRETNA implemented in MATLAB (https://www.nitrc.org/projects/gretna/)[26]. The first 10 volumes of were discarded to achieve magnetization equilibrium. Slice-timing correction was implemented to align the fMRI according to the first slice. The individual images were then realigned so that each part of the brain was in the same position on all volumes and warped into the standard Montreal Neurological Institute (MNI) space. Smoothing was used to improve the signal-to-noise ratio and to attenuate anatomical variances caused by inaccurate inter-subject registration after spatial normalization. Nuisance signals were removed from the time series of each voxel to reduce the effects of non-neuronal fluctuations, including head motion profiles and cerebrospinal fluid and white matter signals. The fMRI data were bandpass-filtered to reduce the effects of low-frequency drift and high-frequency physiological noise. Regions of interest (ROIs) were placed using the automatically labeled template (AAL) brain atlas, which divides the brain into 90 regions. A representative time series from each ROI was obtained by averaging the time series of each voxel within that region. FC was then obtained through Pearson correlation between any possible pairs of ROIs. Fisher's r-to-z transformation was applied to the obtained correlation matrices to improve the normality of the correlation coefficients.

SC network construction

MRtrix3 (https://www.mrtrix.org/) was used to perform fiber tracking. Denoising, Gibbs ringing removal, motion, and distortion corrections were performed as the part of preprocessing. In addition, bias field correction was processed to eliminate low-frequency intensity fluctuations across the image. After preprocessing, the diffusion tensor could be calculated and then the FA metrics could be obtained. The whole-brain fiber tractography was performed in the individual space, which is defined as the cutoff of FA values < 0.2, angle 45°, minimum length 20 mm, and maximum length 200 mm. Anatomic parcellation was performed using AAL. A linear transformation was applied within each subject's DTI and T1WI. The individual T1WI was then nonlinearly registered to the MNI space. Then, the inverse transformation matrix was obtained and applied to the AAL template in standard space. 90 ROIs were used for constructing the SC matrix. A connectivity matrix was obtained by averaging FA by the volume of the fiber tract connecting regions.

Graph theory analysis

Graph theory analysis was performed using the following steps implemented in GRETNA. Each subject has one functional and one structural brain network (90 × 90) (Fig. 1). Only positive connections were retained in graph theoretic calculations. We calculated the small-worldness and nodal degree centrality (DC) for each network. Small-worldness is the ratio of normalized clustering coefficient to average shortest path length. DC is the number of direct connections a node has with other nodes in the network. There is no specific value of FC or SC strength representing the actual relationship between each pair of nodes. Thus, to avoid including extremely spurious connectivity in calculations by applying thresholds in the connectivity matrices, a wide range of sparsity (i.e., 0.10–0.35) with an interval of 0.01 was selected for graph theoretical analysis of brain network to maintain the reachability of the network and allow prominent small-world properties. This sparsity range is widely used to evaluate ensemble network metrics in graph theoretic analysis[27,28]. Then we calculated the area under the curve (AUC) for each network measure to provide a scalar that does not depend on a specific threshold selection. Of note, each network was thresholded to a fixed sparsity value, but retaining the supra-threshold weights.

CBF extracting

The quantitative ASL-CBF map using 1500 ms PLD was generated on an Advantage Windows Workstation using FuncTool software attached to the scanner. ASL data were processed as follows: the ASL images were realigned to correct for head motion; the perfusion difference of images was calculated through sinc subtraction of label/control pairs; spatial smoothing was performed; individual ASL-CBF images were normalized to the T1WI first, and then to the MNI template; normalized ASL-CBF images were overlaid with the AAL template, and the mean CBF value of each ROI was extracted. All registration was performed by ANTS (https://stnava.github.io/ANTs/).

CBF-DC coupling

Previous studies represented NVC with CBF-FC coupling of voxels. FC strength is the degree centrality at the voxel level[29]. At the voxel level, Baller et al. used locally weighted coupling regression coefficient to evaluate the CBF-ALFF coupling, and Wei et al. used the spatial correlation of CBF and FC strength to represent the CBF-FC coupling[12,29]. Similarly, we proposed the CBF-DC coupling to represent NVC at the brain region level, which was calculated as follows. After calculating the CBF and DC for each ROI, at the individual level, we normalized the CBF and DC to z-scores. At the individual level, the whole brain CBF-DC coupling is the spatial correlation coefficient (regression slope) of CBF and DC in all brain regions, and the specific lobe CBF-DC coupling is the coupling regression slope in that lobe. Two-sample t-test was then used to compare CBF-DC coupling between MMD and HC. At the group level, CBF-DC coupling in specific brain region was defined as the correlation of CBF and DC in that region for all individuals in the group[29]. The online platform (http://comparingcorre

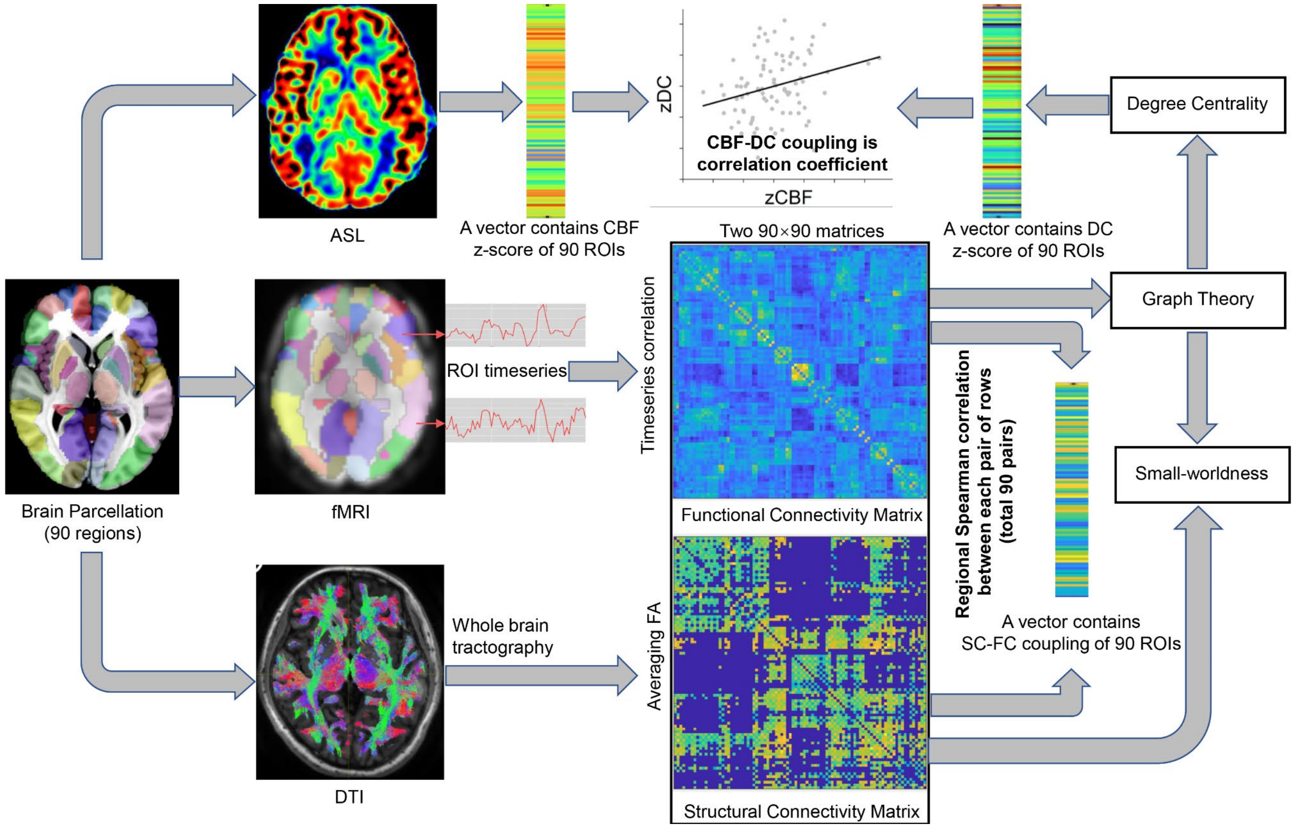

Fig. 1. Schematic overview of the image analysis in this study. The AAL atlas was used to parcellate the brain into 90 ROIs. Based on probabilistic tractography aimed at reconstructing white-matter pathways, the SC matrix was obtained by averaging FA by the volume of the fiber tract connecting regions. The FC matrix was computed by correlating average time series from the defined region pairs. For each individual, we calculated Spearman-rank correlation for each pair of rows (total 90 pairs) in the SC and FC matrix, and then obtained SC-FC coupling of 90 ROIs. Graph theory analyses were performed for FC and SC matrices to calculate small-worldness and DC. For each individual, the CBF and DC of each ROI were normalized into z-scores, and the CBF-DC coupling was the spatial correlation coefficient (regression slope) of regional CBF and DC. *AAL* automatically labeled template, *ROI* region of interest, *SC* structural connectivity, *FA* fractional anisotropy, *FC* functional connectivity, *CBF* cerebral blood flow, *DC* degree centrality.

lations.org) was used to compare the regional CBF-DC coupling between MMD and HC at the group level. Although the previously proposed voxel-based CBF-FC coupling and CBF-ALFF values are more precision[12,29], it is noteworthy that the spatial resolution of ASL used to measure CBF is lower than fMRI. The mismatch in resolution may lead to some decrease in the accuracy of the voxel-based calculation results[12]. Region-based CBF-DC coupling is less precision but may be more accurate and representative.

SC-FC coupling

When obtaining the SC and FC matrices, at the individual level, SC-FC coupling was calculated for each brain region as follows. For each row in SC matrix, representing the SC from one region to other regions, the Spearman-rank correlation with the same row in FC matrix was calculated to obtain SC-FC coupling of 90 brain regions at the individual level[25]. Two-sample t-test was used to compare the regional SC-FC coupling between MMD and HC, and multiple comparisons were corrected by the false discovery rates (FDR). SC-FC coupling in specific lobe was the average of regional SC-FC coupling belong to that lobe.

Statistical analysis

Statistical analyses were performed using SPSS software, version 26.0. Two-sample t test was used to analyze the differences between MMD and HC groups. The pwr package of R-project was used for power analysis. Pearson correlation analysis for normally-distributed data. Multiple comparisons were corrected by the FDR. Specifically, partial correlation was employed with the covariates of age and gender. The threshold for the significance level was set at 0.05.

	MMD ($n=38$)	HC ($n=20$)	*P* value
Age (years) ± SD	45.8 ± 9.2	47.0 ± 4.3	0.536
Gender (female) n (%)	29 (76.3)	14 (70.0)	0.602
Education (years) ± SD	7.9 ± 3.0	9.4 ± 3.1	0.090
Vascular risk factors			
BMI (kg/m^2)	23.56 ± 3.10	23.73 ± 1.21	0.782
Hypertension n (%)	9 (23.7)	3 (15.0)	0.438
Diabetes n (%)	4 (10.5)	0 (0.0)	0.288
Hyperlipemia n (%)	9 (23.7)	3 (15.0)	0.438

Table 1. Demographics in MMD and HC groups. *MMD* moyamoya disease, *HC* healthy control, *BMI* body mass index.

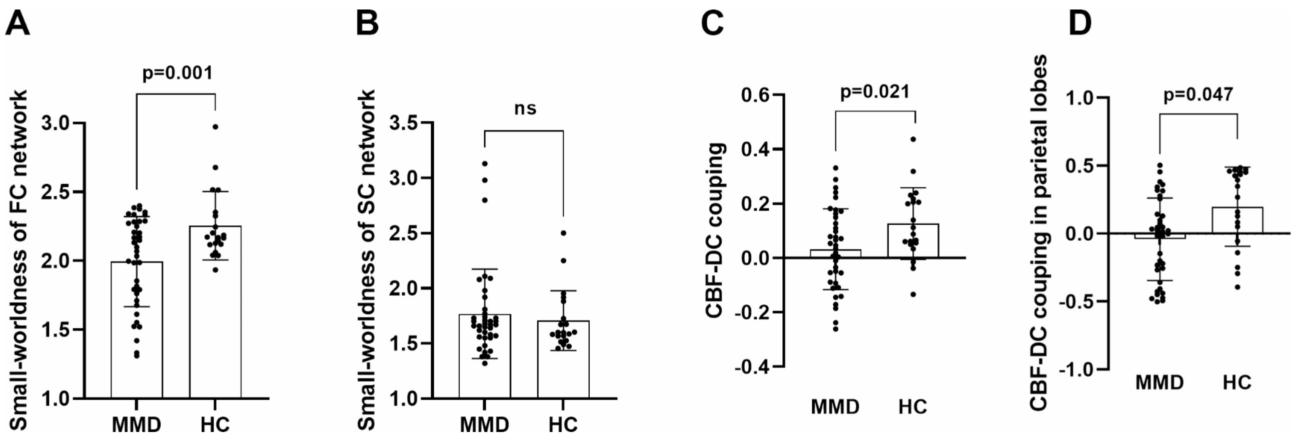

Fig. 2. Network properties and CBF-DC coupling changes in MMD patients. The small-worldness of (**A**) FC and (**B**) SC network, and CBF-DC coupling in the (**C**) whole brain and (**D**) parietal lobe in MMD and HC were exhibited. Bars represent mean ± standard error. *MMD* moyamoya disease, *HC* healthy control, *SC* structural connectivity, *FC* functional connectivity.

Results

Baseline characteristics

38 MMD patients (9 males, 29 females, 45.8 ± 9.2 years old) and 20 healthy subjects (6 males, 14 females, 47.0 ± 4.3 years old) were included in this study. There were also no significant differences in demographic or clinical characteristic between MMD and HC groups (Table 1). Compared with HC, patients with MMD exhibit decreased CBF in the frontal ($p=0.019$), parietal ($p=0.001$), occipital ($p=0.093$), and temporal lobes ($p<0.001$) (Fig. S2). The small-worldness of FC network in MMD decreased ($p=0.001$), while the small-worldness of SC network showed no significant changes (Fig. 2).

CBF-DC coupling in MMD

Compared with HC, CBF-DC coupling was decreased in MMD ($p=0.021$), especially in the parietal lobe ($p=0.047$, FDR corrected) (Fig. 2), where regional CBF-DC coupling was decreased significantly in the right postcentral gyrus, left supramargial gyrus, and right paracentral lobule (Table 2). Power analysis showed a power value of 0.773 for our sample size. Additionally, regional CBF-DC coupling was also decreased in the right middle temporal gyrus and right inferior temporal gyrus, and other brain regions with impaired CBF-DC coupling are shown in Table 2; Fig. 3. CBF-DC coupling was correlated with the small-worldness of SC network ($r=0.371$, $p=0.021$). CBF-DC coupling in the frontal lobe may influence the MoCA scores ($r=0.394$, $p=0.029$, FDR corrected) (Fig. 4). We used multiple linear regression to investigate the factors influencing CBF-DC coupling, and only age showed significance ($\beta=-0.401$, $p=0.028$) (Table S1).

SC-FC coupling in MMD

Analysis based on brain regions showed that SC-FC coupling in MMD decreased in frontal (left dorsolateral superior frontal gyrus, right supplementary motor area), occipital (left and right superior occipital gyrus, right fusiform gyrus), and subcortical regions (left caudate nucleus, right pallidum, left and right thalamus), but increased in temporal lobe (left heschl gyrus, left superior temporal gyrus, left and right temporal pole) (Table 3; Fig. 5). SC-FC coupling at whole brain level was correlated with MMSE scores ($r=0.397$, $p=0.027$, FDR corrected). Further, SC-FC coupling in the frontal lobe was correlated with both MoCA ($r=0.388$, $p=0.030$, FDR corrected) and MMSE scores ($r=0.353$, $p=0.030$, FDR corrected) (Fig. 4). No significant correlation was

Abbr.	Regions	CBF-DC coupling MMD	CBF-DC coupling HC	Z value	*P* value
PreCG.R	Precental gyrus_R	− 0.012	0.353	1.288	0.098
ROL.L	Rolandic operculum_L	− 0.253	0.147	1.375	0.085
SMA.R	Supplementary motor area_R	− 0.151	0.247	1.367	0.085
OLF.L	Olfactory cortex_L	− 0.370	0.228	2.098	0.018*
OLF.R	Olfactory cortex_R	− 0.397	− 0.006	1.400	0.081
ACG.L	Anterior cingulate and paracingulate gyri_L	0.064	0.440	1.380	0.084
PCG.L	Posterior cingulate gyrus_L	− 0.200	0.237	1.503	0.066
PoCG.R	Postcentral gyrus_R	− 0.036	0.423	1.648	0.049*
SMG.L	Supramarginal gyrus_L	− 0.081	0.393	1.679	0.047*
PCUN.L	Precuneus_L	− 0.289	0.140	1.486	0.069
PCL.R	Paracentral lobule_R	− 0.167	0.364	1.860	0.031*
MTG.R	Middle temporal gyrus_R	− 0.385	0.281	2.349	0.009**
ITG.R	Inferior temporal gyrus_R	− 0.165	0.494	2.394	0.008**

Table 2. Regional CBF-DC coupling in MMD and HC groups. Brain regions with a P-value (uncorrected) < 0.1 for the analysis of differences in CBF-DC coupling between groups are listed. *CBF* cerebral blood flow, *DC* degree centrality, *L* left, *R* right. $^{*}p<0.05$, $^{**}p<0.01$.

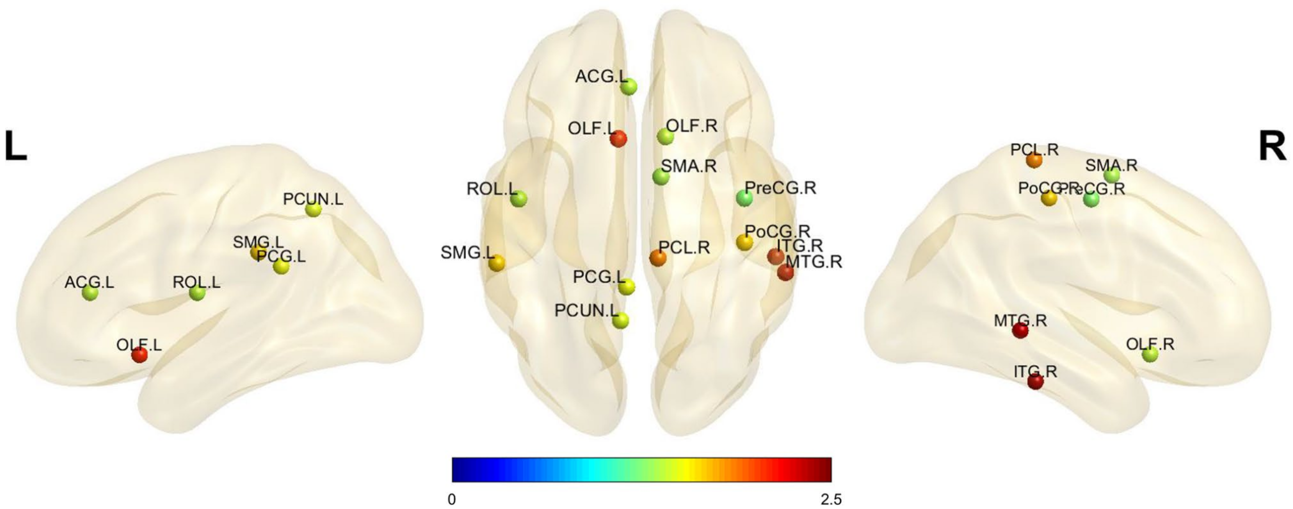

Fig. 3. The distribution of brain regions showing decreased CBF-DC coupling in MMD. Color bar indicates Z-values. Abbreviations and P values corresponding to brain regions are shown in Table 2.

found between SC-FC coupling and CBF. No significant correlation was found between the CBF-DC coupling and SC-FC coupling at the whole-brain level ($r=0.124, p=0.459$) or the frontal level ($r=0.206, p=0.214$). We also investigated factors influencing SC-FC coupling, but no significance was found (Table S2).

Postoperative collateral formation in MMD
Compared with the poor postoperative collateral formation group, CBF-DC coupling was higher in the good postoperative collateral formation group ($p=0.041$) (Table 4). Other clinical characteristics between the two groups showed no significant difference (Table 4).

Discussion
In this study, fMRI, DTI and ASL techniques were used to investigate the NVC and SC-FC coupling changes in MMD patients, and the findings were as follows. NVC decreased in MMD, especially in the parietal lobe. SC-FC coupling decreased in frontal, occipital, and subcortical regions but increased in temporal lobe. NVC was correlated with the small-worldness of SC network and cognitive scores. SC-FC coupling may also influence cognitive scores. Better NVC was found in the good postoperative collateral formation group.

Chronic ischemia and blood flow redistribution in MMD can impact anatomical structural connectivity and physiological functional connectivity, resulting in substantial reconfiguration of cerebral networks. CBF-DC coupling decreased significantly in MMD, indicating a disruption of NVC. At the cellular level, the normal NVC

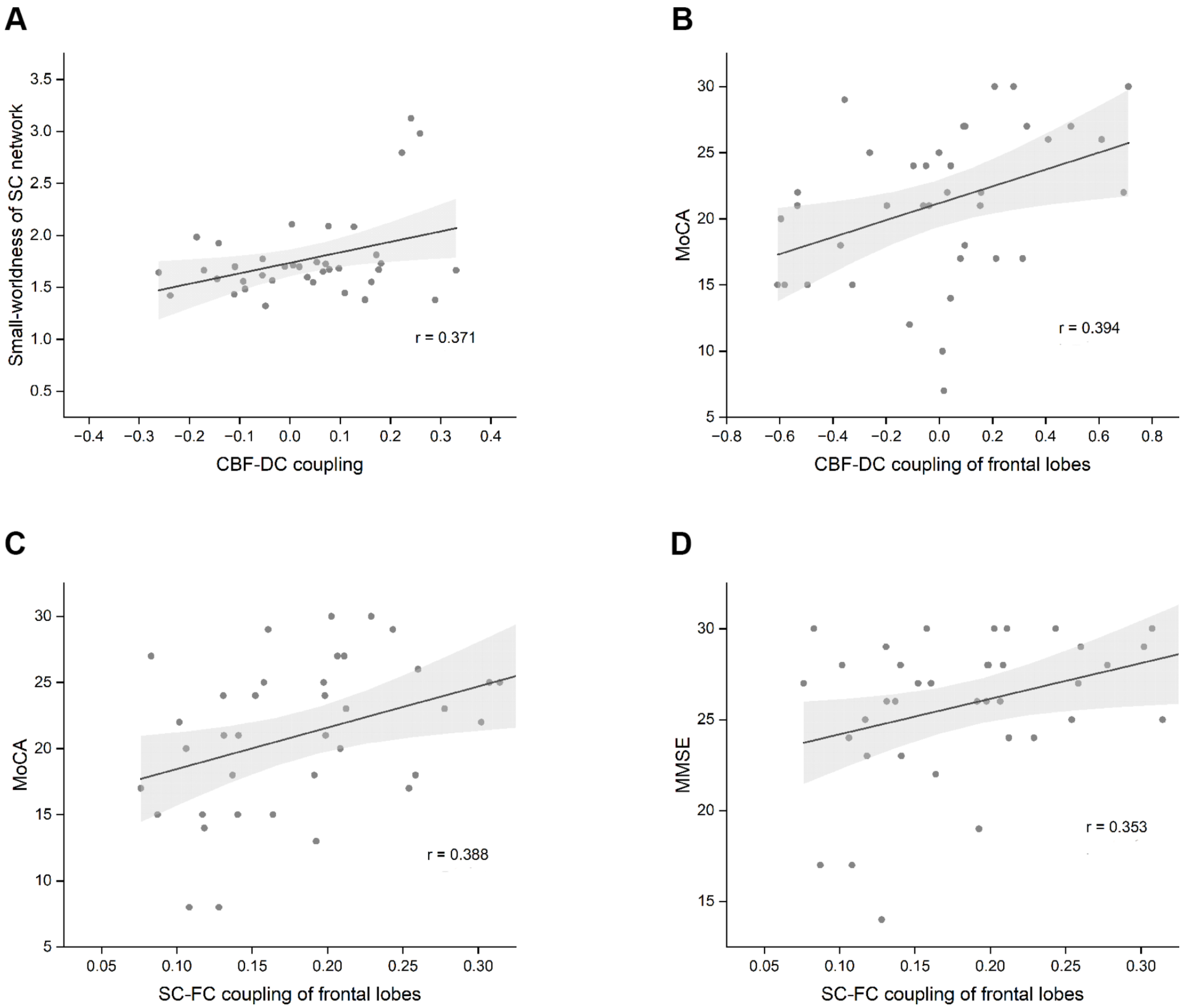

Fig. 4. Correlations of the coupling with small-worldness and cognitive scores in MMD. *MoCA* Montreal cognitive assessment, *MMSE* Mini-Mental State Examination.

process relies on the coordination of astrocytes, where ionic gradients and metabolic byproducts released by activated neurons lead to local vasodilation of cerebral arterioles[16,30]. Suffer from the chronic ischemia in MMD, neuronal structures and ion dynamics undergo gradual adaptations in response to reduced metabolic demand and compromised blood supply, resulting in neurovascular decoupling. On the other hand, endothelial cells with RNF213 variants secrete large quantities of pro-inflammatory cytokines[31], contributing to the occurrence of neuroinflammation, which is a crucial factor influencing NVC[32].

NVC is often observed to be enriched in brain regions with high metabolic activity, such as the frontoparietal neural network that coordinates brain activity across various distributed brain regions[12,33]. The association cortex within the frontoparietal network exhibits larger pyramidal neurons characterized by increased spine and synapse density[34]. These association networks were the most spatially distributed, with more long-distance cortical connections[35]. These neuroanatomical features generate enhanced metabolic activity and, consequently, necessitate a tighter association between neural activity and cerebral perfusion[36]. Notably, impaired CBF, white matter microstructure, and neural activity in MMD frequently manifest in the frontal and parietal lobes[5], thereby impeding the tight but vulnerable NVC within the frontoparietal network. The left supramarginal gyrus serves as a central hub for the execution of complex actions and motor skills, and the postcentral gyrus and paracentral lobule are responsible for processing a majority of the somatic sensory information. According to our findings, NVC of these regions were impaired in MMD.

NVC may also affect the neoangiogenesis following combined bypass surgery. The neoangiogenesis observed after indirect bypass surgery in MMD is deemed unsatisfactory[17]. As previously mentioned, the reduced NVC entails alterations in the microenvironment surrounding neuronal structures, including ionic gradients, metabolites, and neuroinflammatory factors[16,30,32]. This microenvironment is not conducive to the normal function and proliferation of vascular smooth muscle, which will affect the collateral circulation

Abbr.	Regions	SC-FC coupling		T value	q value
		MMD	HC		
SFGdor.L	Superior frontal gyrus, dorsolateral_L	0.006 ± 0.121	0.128 ± 0.149	− 3.08	0.023
SMA.R	Supplementary motor area_R	0.206 ± 0.137	0.299 ± 0.095	− 2.98	0.038
SFGmed.R	Superior frontal gyrus, medial_R	0.266 ± 0.137	0.168 ± 0.098	2.78	0.048
DCG.L	Median cingulate and paracingulate gyri_L	0.147 ± 0.133	0.256 ± 0.143	− 2.83	0.038
SOG.L	Superior occipital gyrus_L	0.240 ± 0.154	0.337 ± 0.096	− 2.93	0.038
SOG.R	Superior occipital gyrus_R	0.221 ± 0.128	0.328 ± 0.054	− 4.42	0.005
FFG.R	Fusiform gyrus_R	0.187 ± 0.175	0.324 ± 0.109	− 3.63	0.013
CAU.L	Caudate nucleus_L	0.145 ± 0.129	0.250 ± 0.153	− 2.74	0.048
PAL.R	Lenticular nucleus, pallidum_R	0.097 ± 0.170	0.201 ± 0.114	− 2.73	0.048
THA.L	Thalamus_L	0.129 ± 0.166	0.233 ± 0.100	− 2.94	0.038
THA.R	Thalamus_R	0.105 ± 0.181	0.221 ± 0.067	− 3.47	0.013
HES.L	Heschl gyrus_L	0.179 ± 0.156	0.021 ± 0.124	3.85	0.009
STG.L	Superior temporal gyrus_L	0.194 ± 0.170	0.055 ± 0.086	4.09	0.005
TPOsup.L	Temporal pole: superior temporal gyrus_L	0.235 ± 0.185	0.098 ± 0.105	3.55	0.013
TPOsup.R	Temporal pole: superior temporal gyrus_R	0.237 ± 0.126	0.108 ± 0.115	3.74	0.009

Table 3. Regional SC-FC coupling in MMD and HC groups. *q*-values are FDR-corrected *p*-values. *SC* structural connectivity, *FC* functional connectivity, *L* left, *R* right.

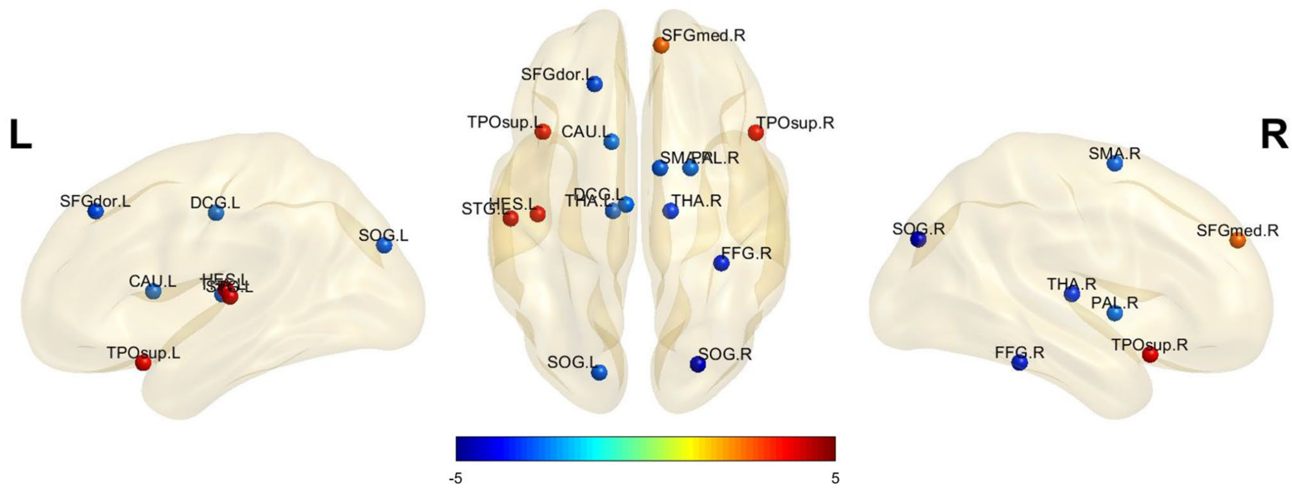

Fig. 5. The distribution of brain regions showing altered SC-FC coupling in MMD. Color bar indicates T-values, and blue means decrease, red means increase. Abbreviations and q values corresponding to brain regions are shown in Table 3.

formation after vascular reconstruction in MMD[17]. These alterations are challenging to rectify within a short timeframe and can impede the neoangiogenesis. Higher NVC also represented a mutually supportive relationship between neuronal activity and blood supply. The direct bypass of the combined bypass surgery provided an immediate improvement of blood perfusion in the ischemic brain area, which will promote the recovery of neuronal function. With enhanced neuronal activity, the demand for blood supply also increased, stimulating neoangiogenesis in the indirect revascularization, which was a positive feedback process. According to the hypothesis of Duan et al., the stimulation of ischemia, that is, the increase in hemodynamic demand, was the main influencing factor for good collateral formation after indirect revascularization in MMD[37]. Previous studies showed that preoperative collateral circulation grade, age, hemorrhage, diabetes and hyperlipemia associated with postoperative neoangiogenesis[17,38,39]. Due to the limited sample size in this study, some of the aforementioned factors exhibited a trend of intergroup differences, but not statistically significant.

Alterations in vascular phenotype and hemodynamics will progressively disturb the neurovascular dynamic balance, resulting in mild cognitive decline[18,40]. The onset of stroke precipitates a rapid deterioration in NVC, frequently accompanied by profound cognitive impairment[18]. Neurovascular uncoupling means that neuronal activity is no longer associated with spontaneous cerebral hemodynamic regulation. Without hemodynamic regulation, neuronal activity may be disordered and meaningless, leading to neurocognitive impairment. The correlation between NVC in frontal lobes and cognitive performance is in line with the observed tendency

	Poor collateral formation ($n=16$)	Good collateral formation ($n=22$)	P value
Age (years) ± SD	46.2 ± 7.9	45.6 ± 10.3	0.705
Gender (female) n (%)	10 (62.5)	19 (86.4)	0.088
Vascular risk factors			
BMI (kg/m^2)	23.57 ± 3.25	23.53 ± 2.99	0.969
Hypertension n (%)	4 (25.0)	5 (22.7)	0.871
Diabetes n (%)	2 (12.5)	2 (9.1)	0.735
Hyperlipemia n (%)	2 (12.5)	7 (31.8)	0.167
Hemorrhage n (%)	9 (56.3)	7 (31.8)	0.132
Suzuki stage, median (IQR)	3 (2–3)	2.5 (1.75–4)	0.172
CBF-DC coupling ± SD	− 0.02 ± 0.12	0.08 ± 0.16	0.041
SC-FC coupling ± SD	0.17 ± 0.04	0.19 ± 0.05	0.130

Table 4. Clinical characteristics in poor and good collateral formation groups. *CBF* cerebral blood flow, *DC* degree centrality, *SC* structural connectivity, *FC* functional connectivity.

for functional impairment to manifest predominantly in frontal lobes of MMD patients[5]. Furthermore, the association between impaired small-worldness of structural networks and reduced NVC was found. Indeed, myelin changes in white matter can impact NVC[24,25]. Oligodendrocytes deliver metabolic substrates to neurons through myelin sheath, and this additional metabolic support along axons contributes to the maintenance of proper neuronal function[41]. Importantly, axons responsible for long-distance cortical connections in association cortices such as the frontoparietal network tend to be myelinated[42]. When the integrity of myelin sheath is impaired, the neuronal soma may experience insufficient metabolic support to generate an equivalent nerve impulse. Engaging the same neural activity would necessitate reduced CBF, leading to a decline in NVC[12]. The above results suggest that cerebral neurovascular decoupling may be the pathophysiological mechanism of MMD.

SC-FC coupling represents the level of concordance between the anatomical structural connectomes and physiological functional connectomes in brain, elucidating the functional dynamics in terms of structural topology[22]. Wang et al. proposed that perturbations in the optimal structural organization could result in diminished functional dynamics[43]. The SC between brain regions ensures the transmission of neuronal electrical signal along axons and strengthens the connection of functional activities. However, chronic ischemia in MMD may impair microstructural connectivity[5], resulting in decreased activity synchrony among brain regions responsible for the similar cognitive function domain. Thus, SC-FC decoupling can impair neurocognitive function, which has been found in various neurological diseases such as stroke and alzheimer disease (AD)[22,44]. Gu et al. proposed that SC-FC coupling exhibited significant variation across different brain regions, but it was particularly robust in visual and subcortical areas characterized by high levels of structural connectivity[21].

Similarly, SC-FC coupling in occipital and subcortical regions was significantly impaired in MMD, indicating that these highly connected nodes are more vulnerable and susceptible[45]. Besides, several studies have consistently reported decreased functional activity in the dorsolateral superior frontal gyrus, a key region of the central executive network, in MMD patients[2,3]. SC-FC coupling analysis can provide complementary insights into these neuropathological alterations. Decreased SC-FC coupling in the supplementary motor area could potentially signify an underlying motor function deficit in MMD. Conversely, heightened SC-FC coupling within the temporal lobe might serve as a compensatory mechanism to uphold language, emotion, and memory functions. The association between SC-FC coupling and diverse cognitive functions can exhibit variation across distinct brain regions and populations[21]. Specifically, enhanced SC-FC coupling in the prefrontal cortex is notably linked to the development of executive function[25]. The disruption of structure-function relationship in AD is considered a primary contributor to cognitive dysfunction[46]. The progressive degeneration of brain structures, such as the hippocampus and cortical regions, leads to impaired functional connectivity and subsequent cognitive deficits. Similarly, impaired frontal SC-FC coupling in MMD is associated with cognitive impairment. The decreased blood flow in the frontal regions, characteristic of MMD, may disrupt the structure-function relationship and cognitive performance.

Regarding limitations, first, we enrolled MMD patients without visible lesions on T1WI, so the conclusions were not applicable to all MMD patients. Second, both CBF and DC are indirect measures of vascular and neuronal function in brain regions, and this region-based coupling is less precision than the voxel-based coupling. Third, we used only a single PLD to calculate CBF, but methods using longer PLD or multiple PLD were able to reflect CBF more accurately. Techniques such as deconvolution can help in separating arterial transit time effects from true tissue perfusion. Last, the sample size of our current study is relatively small and all patients were enrolled from a single-center, so a potential selection bias towards regions and races may have occurred. Thus, our findings may not be conclusive. In the future, we need to expand the sample size and explore the advantages and disadvantages of different NVC measures.

Conclusions

In conclusion, we observed changes in NVC and SC-FC coupling in MMD by combining fMRI, DTI, and ASL techniques. The NVC decreased in MMD, particularly in the parietal lobe. SC-FC coupling decreased in frontal, occipital, and subcortical regions but increased in temporal lobe. NVC has exhibited correlations with the small-worldness of structural network and cognitive scores. SC-FC coupling may also impact cognitive scores. Better NVC was found in the good postoperative collateral formation group. Neurovascular decoupling and structure-functional decoupling at the cortical level may be the underlying neuropathological mechanisms of MMD.

Data availability

The data that support the findings of this study are available from the corresponding author upon reasonable request.

Received: 15 June 2024; Accepted: 9 December 2024
Published online: 28 December 2024

References

1. Ihara, M. et al. Moyamoya disease: diagnosis and interventions. *Lancet Neurol.* **21** (8), 747–758 (2022).
2. Lei, Y. et al. Postoperative executive function in adult moyamoya disease: a preliminary study of its functional anatomy and behavioral correlates. *J. Neurosurg.* **126** (2), 527–536 (2017).
3. Lei, Y. et al. Aberrant regional homogeneity of resting-state executive control, default mode, and salience networks in adult patients with moyamoya disease. *Brain Imaging Behav.* **11** (1), 176–184 (2017).
4. Sakamoto, Y. et al. Default Mode Network changes in Moyamoya Disease before and after bypass surgery: preliminary Report. *World Neurosurg.* **112**, e652–e661 (2018).
5. Kazumata, K. et al. Chronic ischemia alters brain microstructural integrity and cognitive performance in adult moyamoya disease. *Stroke* **46** (2), 354–360 (2015).
6. Kazumata, K. et al. Combined structural and diffusion tensor imaging detection of ischemic injury in Moyamoya disease: relation to disease advancement and cerebral hypoperfusion. *J. Neurosurg.* **134** (3), 1155–1164 (2020).
7. Hu, J. et al. Moyamoya Disease with initial ischemic or hemorrhagic attack shows different brain structural and functional features: a pilot study. *Front. Neurol.* **13**, 871421 (2022).
8. Sun, Y., Li, J., Suckling, J. & Feng, L. Asymmetry of Hemispheric Network Topology reveals dissociable processes between functional and structural brain connectome in Community-Living elders. *Front. Aging Neurosci.* **9**, 361 (2017).
9. Griffa, A., Baumann, P. S., Thiran, J. P. & Hagmann, P. Structural connectomics in brain diseases. *Neuroimage* **80**, 515–526 (2013).
10. Kazumata, K. et al. Investigating Brain Network characteristics interrupted by Covert White Matter Injury in patients with Moyamoya Disease: insights from Graph Theoretical Analysis. *World Neurosurg.* **89**, 654–665e2 (2016).
11. He, S. et al. Impairments in brain perfusion, executive control network, topological characteristics, and neurocognition in adult patients with asymptomatic Moyamoya disease. *BMC Neurosci.* **22** (1), 35 (2021).
12. Baller, E. B. et al. Developmental coupling of cerebral blood flow and fMRI fluctuations in youth. *Cell. Rep.* **38** (13), 110576 (2022).
13. Segarra, M., Aburto, M. R., Hefendehl, J. & Acker-Palmer, A. Neurovascular interactions in the nervous system. *Annu. Rev. Cell. Dev. Biol.* **35**, 615–635 (2019).
14. Satterthwaite, T. D. et al. Impact of puberty on the evolution of cerebral perfusion during adolescence. *Proc. Natl. Acad. Sci. USA*. **111** (23), 8643–8648 (2014).
15. Liu, F. et al. Resting state cerebral blood flow with arterial spin labeling MRI in developing human brains. *Eur. J. Paediatr. Neurol.* **22** (4), 642–651 (2018).
16. Takano, T. et al. Astrocyte-mediated control of cerebral blood flow. *Nat. Neurosci.* **9** (2), 260–267 (2006).
17. Gao, G. et al. Factors influencing collateral circulation formation after Indirect Revascularization for Moyamoya Disease: a Narrative Review. *Transl Stroke Res.* (2023).
18. Girouard, H. & Iadecola, C. Neurovascular coupling in the normal brain and in hypertension, stroke, and Alzheimer disease. *J. Appl. Physiol. (1985)*. **100** (1), 328–335 (2006).
19. Presa, J. L., Saravia, F., Bagi, Z. & Filosa, J. A. Vasculo-neuronal coupling and neurovascular coupling at the neurovascular unit: impact of hypertension. *Front. Physiol.* **11**, 584135 (2020).
20. Mišić, B. et al. Network-level structure-function relationships in human neocortex. *Cereb. Cortex*. **26** (7), 3285–3296 (2016).
21. Gu, Z., Jamison, K. W., Sabuncu, M. R. & Kuceyeski, A. Heritability and interindividual variability of regional structure-function coupling. *Nat. Commun.* **12** (1), 4894 (2021).
22. Cao, R. et al. Abnormal Anatomical Rich-Club Organization and structural-functional coupling in mild cognitive impairment and Alzheimer's Disease. *Front. Neurol.* **11**, 53 (2020).
23. Medaglia, J. D. et al. Functional alignment with Anatomical Networks is Associated with Cognitive Flexibility. *Nat. Hum. Behav.* **2** (2), 156–164 (2018).
24. Paquola, C. et al. Shifts in myeloarchitecture characterise adolescent development of cortical gradients. *Elife* **8**, 1 (2019).
25. Baum, G. L. et al. Development of structure-function coupling in human brain networks during youth. *Proc. Natl. Acad. Sci. U S A*. **117** (1), 771–778 (2020).
26. Wang, J. et al. GRETNA: a graph theoretical network analysis toolbox for imaging connectomics. *Front. Hum. Neurosci.* **9**, 386 (2015).
27. He, Y. et al. Uncovering intrinsic modular organization of spontaneous brain activity in humans. *PLoS One*. **4** (4), e5226 (2009).
28. Achard, S. & Bullmore, E. Efficiency and cost of economical brain functional networks. *PLoS Comput. Biol.* **3** (2), e17 (2007).
29. Wei, W., Wang, T., Abulizi, T., Li, B. & Liu, J. Altered coupling between resting-state cerebral blood Flow and Functional Connectivity Strength in Cervical Spondylotic Myelopathy patients. *Front. Neurol.* **12**, 713520 (2021).
30. Blanco, V. M., Stern, J. E. & Filosa, J. A. Tone-dependent vascular responses to astrocyte-derived signals. *Am. J. Physiol. Heart Circ. Physiol.* **294** (6), H2855–H2863 (2008).
31. Roy, V. et al. Moyamoya Disease susceptibility gene RNF213 regulates endothelial barrier function. *Stroke* **53** (4), 1263–1275 (2022).
32. Nedeljkovic, N. Complex regulation of ecto-5'-nucleotidase/CD73 and A(2A)R-mediated adenosine signaling at neurovascular unit: a link between acute and chronic neuroinflammation. *Pharmacol. Res.* **144**, 99–115 (2019).
33. Passow, S. et al. Default-mode network functional connectivity is closely related to metabolic activity. *Hum. Brain Mapp.* **36** (6), 2027–2038 (2015).
34. Beul, S. F. & Hilgetag, C. C. Neuron density fundamentally relates to architecture and connectivity of the primate cerebral cortex. *Neuroimage* **189**, 777–792 (2019).
35. Bazinet, V., Vos de Wael, R., Hagmann, P., Bernhardt, B. C. & Misic, B. Multiscale communication in cortico-cortical networks. *Neuroimage* **243**, 118546 (2021).
36. Shokri-Kojori, E. et al. Correspondence between cerebral glucose metabolism and BOLD reveals relative power and cost in human brain. *Nat. Commun.* **10** (1), 690 (2019).
37. Liu, Z. W. et al. Collateral circulation in Moyamoya disease: a new grading system. *Stroke* **50** (10), 2708–2715 (2019).

38. He, Q. et al. Hyperhomocysteinemia is a predictor for poor postoperative angiogenesis in adult patients with moyamoya disease. *Front. Neurol.* **13**, 902474 (2022).
39. Ren, B. et al. Surgical outcomes following encephaloduroarteriosynangiosis in adult moyamoya disease associated with type 2 diabetes. *J. Neurosurg.* **125** (2), 308–314 (2016).
40. Garrett, D. D., Lindenberger, U., Hoge, R. D. & Gauthier, C. J. Age differences in brain signal variability are robust to multiple vascular controls. *Sci. Rep.* **7** (1), 10149 (2017).
41. Stadelmann, C., Timmler, S., Barrantes-Freer, A. & Simons, M. Myelin in the Central Nervous System: structure, function, and Pathology. *Physiol. Rev.* **99** (3), 1381–1431 (2019).
42. Váša, F. et al. Adolescent Tuning of Association Cortex in Human Structural Brain Networks. *Cereb. Cortex.* **28** (1), 281–294 (2018).
43. Wang, J. et al. Alterations in brain network topology and structural-functional connectome coupling relate to cognitive impairment. *Front. Aging Neurosci.* **10**, 404 (2018).
44. Chen, H. et al. Alterations of brain network topology and structural connectivity-functional connectivity coupling in capsular versus pontine stroke. *Eur. J. Neurol.* **28** (6), 1967–1976 (2021).
45. Rubinov, M. & Sporns, O. Complex network measures of brain connectivity: uses and interpretations. *Neuroimage* **52** (3), 1059–1069 (2010).
46. Qiu, Y. et al. Inter-hemispheric functional dysconnectivity mediates the association of corpus callosum degeneration with memory impairment in AD and amnestic MCI. *Sci. Rep.* **6**, 32573 (2016).

Acknowledgements

This study was supported by grants from the National Natural Science Foundation of China provided the funding for this work (NO. 81870910 and 82171271), as well as the Key Research and Development Program of Zhejiang Province (No. 2022C03133).

Author contributions

L.W. and R.B. contributed to the study conception and design. Material preparation and data collection were performed by J.H., Y.L and Y.Z. Data analysis was performed by L.J. and X.H. The first draft of the manuscript was written by L.J. and all authors commented on previous versions of the manuscript. All authors read and approved the final manuscript.

Declarations

Competing interests

The authors declare no competing interests.

Ethical approval

The study was conducted in accordance with the principles of the Declaration of Helsinki and was approved by the Human Research Ethics Committee of Second Affiliated Hospital of Zhejiang University (ID: 2020-064). Informed consent was obtained from each subject.

Additional information

Supplementary Information The online version contains supplementary material available at https://doi.org/10.1038/s41598-024-82729-5.

Correspondence and requests for materials should be addressed to L.W.

Reprints and permissions information is available at www.nature.com/reprints.

Publisher's note Springer Nature remains neutral with regard to jurisdictional claims in published maps and institutional affiliations.